IOP Publishing Physica Scripta
Phys. Scr. **95** (2020) 035208 (8pp) https://doi.org/10.1088/1402-4896/ab501e

Performance improvements and parametric design strategies of an updated thermionic-photovoltaic converter

Wangyang Li, Wanli Peng, Zhimin Yang, Guozhen Su[1], Shanhe Su[1] and Jincan Chen

Engineering Research Center of Micro-Nano Optoelectronic Materials and Devices, Ministry of Education, Fujian Key Laboratory of Semiconductors and Applications, CI Center for OSED, and Department of Physics, Xiamen University, Xiamen 361005, People's Republic of China

E-mail: gzsu@xmu.edu.cn and shanhesu@xmu.edu.cn

Received 23 July 2019, revised 10 October 2019
Accepted for publication 22 October 2019
Published 4 February 2020

Abstract

A novel model of the hybrid converter consisting of a thermionic generator with a graphene-based anode and a photovoltaic (PV) cell is proposed. The power output densities and efficiencies of two single subsystems and the hybrid converter are derived. The effects of the emitter temperature, voltage outputs, and band gap energy on the performance of the hybrid converter are analyzed. The optimally operating bounds of several critical parameters including the power output density, efficiency, and voltage outputs of the hybrid converter are determined. It is found that in the optimally working region, the performance of the hybrid converter with a graphene-based anode is obviously better than that with a metallic anode. It is also found that in a certain temperature range, the maximum efficiency and power output density of the hybrid converter significantly exceed those of the thermionic generator or PV cell.

Keywords: thermionic generator, thermophotovoltaic cell, graphene-based anode, hybrid converter, performance optimization, parametric design

(Some figures may appear in colour only in the online journal)

Nomenclature

A^*	Richardson–Dushman constant, A cm^{-2} K^2
e	elementary charge, C
E	total energy of electrons, eV
E_c	cut off energy, eV
E_g	band gap energy, eV
E_p	parallel energy of electrons, eV
E_x	normal energy of electrons, eV
j_e	forward current density, A cm^{-2}
j_g	reverse current density, A cm^{-2}
j_{TIG}	current density of TIG, A cm^{-2}
j_{TPV}	current density of TPV cell, A cm^{-2}
k_B	Boltzmann constant, J K^{-1}
k_p	wave vector of parallel component
k_x	wave vector of normal component
m	mass of an electron, kg
P	power output density of TIPV converter, W cm^{-2}
P_{TIG}	power output density of TIG, W cm^{-2}
P_{TPV}	power output density of TPV cell, W cm^{-2}
Q_e	energy flux of electrons, W cm^{-2}
Q_h	energy flux of photons, W cm^{-2}
Q'_h	energy flux of photons in TIG, W cm^{-2}
T_e	temperature of emitter, K

[1] Authors to whom any correspondence should be addressed.

 © 2020 IOP Publishing Ltd Printed in the UK

T_c	temperature of PV cell, K
ν_f	velocity of massless Dirac fermions, cm s^{-1}
ν_x	velocity of massless Dirac fermions, cm s^{-1}
V_1	voltage output of TIG, V
V_2	voltage output of TPV cell, V

Greek letter

φ_c	work function of collector, eV
φ_e	work function of emitter, eV
μ	chemical potential, eV
$\hbar$	reduced Planck constant J s
ρ	number of electron states
η	efficiency of TIPV converter
η_{TIG}	efficiency of TIG
η_{TPV}	efficiency of TPV cell

Subscript

max	maximum
min	minimum

Abbreviation

TIG	thermionic generator
TIPV	thermionic generator-photovoltaic
TPV	thermophotovoltaic

1. Introduction

In order to increase the power output density of thermophotovoltaic (TPV) cells, a hybrid thermionic generator-photovoltaic (TIPV) converter [1] has been established to replace a single thermionic generator (TIG) or TPV cell. The TIPV converter combines the TIG and TPV cell into an integral solid-state device. It mainly consists of an emitter, a collector, and a photovoltaic (PV) cell [1]. The emitter simultaneously radiates electrons and photons, enabling the heat transfer to be enhanced and boosting the power output density of the TIPV converter [1]. Donald *et al* fabricated a TIPV device by combining the cesium vapor TIG with silicon and gallium arsenide PV cell [2]. Robert *et al* used a combination of dye-sensitized solar cell and TIG to design efficient electric power converters [3]. The collector is an important component for the TIPV converter, which should have high optical transparency to ensure that photons are absorbed by the PV cell and low work function to ensure the high voltage output of the TIG [4–7]. The possible transparent collectors include very thin metallic layers on sappire [8–10], metallic grids, low work function transparent conducting oxides [9, 10], or negative electron affinity semiconductor [11–13]. Although some metals with relatively low work functions have been explored, such as LaB_6 heterostructure, whose work function is around 2–3 eV [14], most metal materials have disadvantages of low optical transmittance in the range of 20%–40% [15]. Exploring the collector with high optical transmittance and low work function is a main challenge for TIPV converters. The application of graphene offers an alternative way to overcome such problems. The optical transmittance of single-layer graphene can reach up to 97%–98% and the reflectance of graphene is less than 0.1% [8–10]. The work function of graphene can be adjusted [11–13] and has been reduced to 1.69 eV [16].

As a solid state heat engine, the TIG can directly convert a part of heat into electric energy without moving parts. It is mainly composed of a high temperature emitter and a low temperature collector separated by a vacuum gap [8, 9]. The development of the TIG is obstructed by highly operating temperatures and the high work function of practical materials [1]. Owing to the excellent performances of graphene, it may be a suitable candidate for the electrode materials of the TIG. Liang and Ang [17] studied the thermionic emission from singly-layer graphene and explored monolayer graphene as the cathode material of the TIG. Zhang *et al* [18] optimized the concentrated solar TIG with monolayer graphene-based emitter and the results showed that the performance of the TIG with the graphene-based cathode is better than that of the TIG with the metallic cathode. A prototype TIG was demonstrated by Yuan *et al* [16] to use firstly back-gated graphene anode and reduced the work function of graphene from 1.85 to 1.69 eV. Furthermore, Yuan *et al* [19] first experimentally achieved graphene with ultra-low work functions near 1 eV via the approaches of electrostatic gating and Cs/O surface coating. The pervious works indicated that graphene may be a suitable material for the collector of the TIPV converter.

The rest of this paper is organized as follows. In section 2, an updated model of the TIPV converter with a graphene-based anode is established. The structure and working principle of the model are briefly described. In section 3, we obtain the expressions of the power output and efficiency of the converter. In section 4, numerical studies are carried out so that the optimally operating regions of several critical parameters and the maximum power output density and efficiency are determined. The performance characteristics between the TIPV converters with the graphene-based anode and the metallic anode [1] are compared. The conclusions are given in section 5.

2. An updated model of the TIPV converter

Figure 1 schematically shows a TIPV converter consisting of four elements: an emitter, a graphene-based collector, a filter, and a TPV cell. Although figure 1 is similar to the schematic of the TIPV converter proposed by Datas [1], a graphene-based collector is used to replace the metallic anode in [1] and a filter is placed between the collector and the TPV cell. In figure 1, the emitter is made of metallic material and heated to a sufficiently high temperature to radiate photons and high-energy electrons. The emitter and the collector are separated by a vacuum gap. The emitted electrons with high-enough

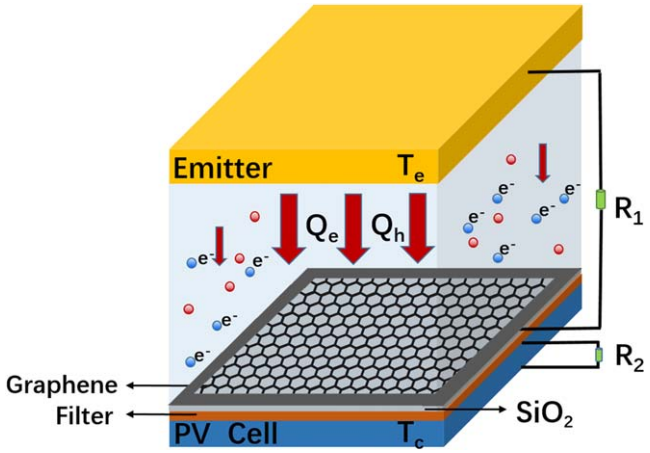

Figure 1. The schematic diagram of a TIPV converter.

energy can overcome the potential barrier and over the vacuum gap. The TIG utilizes a single-layer graphene as the collector material. The collector captures these electrons, which are transmitted to the emitter through the external load. The electron transfer in the TIG is not affected by the filter placed between the anode and the PV cell. In reality, the selective filter can be implemented by various approaches, and filters may be sometimes attached on top of the TPV to save space [20]. Metallic meshes is the original filter, such as 2D periodic copper grid arrays with square, circular-loop, and cross apertures on thin dielectric films [21]. The cascaded inhomogeneous dielectric substrates are considered as the most promising candidates for optical filter [22], such as 1D Si/SiO_2 photonic crystals [22] and 1D metallic-dielectric (Ag/SiO_2) photonic crystal [23], and the performance of TPV can be significantly improved [22]. It is noted that the graphene-based anode including the silicon dioxide (SiO_2) layer has favorable optical properties for light transmission. Thus, the optical selection is implemented by the energy filter. The emitted photons flow through the transparent graphene layer and SiO_2 layer. Those photons with energies above the cut off energy E_c traverse through the filter, and the TPV cell converts the photons with energy greater than the band gap (E_g) of the TPV into electricity, whereas the photons with energies below the cut-off energy E_c are reflected by the filter and absorbed by the emitter. The circuits of the TIG and TPV cell are connected independently. In figure 1, V_1 and V_2 are the voltage outputs of the TIG and TPV cell, and T_e and T_c represent the temperatures of the emitter and the TPV cell. For simplification, it is assumed that the graphene-based collector and the TPV cell are at the same temperature. Because of the low temperature and high thermal conductivity of graphene [24], the lateral conduction through a single graphene layer is not considered by assuming that the graphene layer has a uniform temperature distribution.

3. The power output density and efficiency

The electron state of the graphene is described by a two-component wave function. In the low-energy regime, the energy dispersion of the parallel component exhibits $E_p = \hbar v_f |k_p|$, while that of the normal component takes the form of $E_x = \hbar^2 k_x^2/(2m)$, where v_f is the velocity of massless Dirac fermions [17, 18, 25–28], k_p and k_x are, respectively, the wave vectors of parallel and normal components, $\hbar$ denotes the reduced Planck constant, and m denotes the mass of an electron.

The number of electron states per unit cell with the parallel energy between E_p and $E_p + \mathrm{d}E_p$ and the normal energy between E_x and $E_x + \mathrm{d}E_x$ can be derived as [17, 28]

$$\rho(E_p, E_x)\mathrm{d}E_p\mathrm{d}E_x = \frac{E_p}{2\pi^2\hbar^3 v_f^2}\sqrt{\frac{m}{2E_x}}\mathrm{d}E_p\mathrm{d}E_x, \tag{1}$$

where the spin degeneracy of electron is set to be equal to 2. The occupation probability of an electron state with the total energy E is described by the Fermi–Dirac (FD) distribution function $f_{\mathrm{FD}}(E) = \{1 + \exp[(E-\mu)/(k_\mathrm{B}T_c)]\}^{-1}$, where k_B is the Boltzmann constant, and μ is the chemical potential.

The number of electrons flowing out of the graphene plane with the parallel energy between E_p and $E_p + \mathrm{d}E_p$ and the normal energy between E_x and $E_x + \mathrm{d}E_x$ per unit area and per unit time is given by

$$\rho(E_p, E_x)f_{\mathrm{FD}}(E)v_x\mathrm{d}E_p\mathrm{d}E_x = \frac{E_p}{2\pi^2\hbar^3 v_f^2}f_{\mathrm{FD}}(E)\mathrm{d}E_p\mathrm{d}E_x, \tag{2}$$

where $v_x = \sqrt{2E_x/m}$ is the velocity of electron along the direction perpendicular to the graphene plane. By using equation (2), the current density of electrons with the normal energy between E_x and $E_x + \mathrm{d}E_x$ is given by

$$\begin{aligned} N(E_x)\mathrm{d}E_x &= \frac{\mathrm{d}E_x}{2\pi^2\hbar^3 v_f^2}\int_{E_x}^{\infty}(E - E_x)f_{\mathrm{FD}}(E)\mathrm{d}E \\ &= \frac{(k_\mathrm{B}T_c)^2\mathrm{d}E_x}{2\pi^2\hbar^3 {v_f}^2}f_2(Z_1), \end{aligned} \tag{3}$$

where $f_l(Z_1) = \frac{1}{\Gamma(l)}\int_0^\infty \frac{x^{l-1}}{1+Z_1^{-1}e^x}\mathrm{d}x$ is the Fermi integral, $\Gamma(l)$ is the Gamma function, and $Z_1 = \mathrm{e}^{-(E_x-\mu)/k_\mathrm{B}T_c}$.

Therefore, the current density of the electrons from the collector emitting along the direction perpendicular to the graphene plane is expressed as

$$j_g = \int_{\varphi_c}^{\infty} eN(E_x)\mathrm{d}E_x = \frac{(k_\mathrm{B}T_c)^2}{2\pi^2\hbar^3 {v_f}^2}e\int_{\varphi_c}^{\infty} f_2(Z_1)\mathrm{d}E_x, \tag{4}$$

where e is the elementary positive charge, and φ_c is the work function of the collector.

The current density emitted from the emitter at temperature T_e is given by the Richardson–Dushman equation [17], i.e.

$$j_e = A^* T_e^2 \exp(-\varphi_e/k_\mathrm{B}T_e), \tag{5}$$

where $A^* = 4\pi m k_\mathrm{B}^2 e/h^3 \approx 120\ \mathrm{A\ cm^{-2}\ K^2}$ is Richardson's constant. φ_e is the work function of the emitter. When the space charge effect in the vacuum gap is ignored and the potential distribution is assumed to be flat, the voltage output of the TIG can be defined as $V_1 = (\varphi_e - \varphi_c)/e$. Generally, with the space charge effect, the voltage output is defined as the difference of the electrodes' Fermi levels [29]. In the

presence of the space charge effect, φ_c and φ_e in equations (4) and (5) should be conceived as the differences between the potential maximum in the gap and the Fermi levels of electrodes, respectively. By ignoring the space charge effect and the positive ion emission from the emitter, the net current density of the ideal TIG can be expressed as

$$j_{\mathrm{TIG}} = j_e - j_g. \tag{6}$$

To evaluate the performance of the TIPV converter, we adopt the following assumptions: The cell runs at the radiative limit, where the radiative recombination is the only loss mechanism; the photons with energy greater than the band gap E_g of the PV cell are absorbed by the PV cell and converted into electrical energy [30, 31]. Thus, the net current density of the TPV cell can be expressed as [1, 3, 32–36]

$$j_{\mathrm{TPV}} = \frac{2\pi e}{h^3c^2}\left[\int_{E_g}^{\infty}\frac{E^2}{\exp[E/k_{\mathrm{B}}T_e]-1}\mathrm{d}E - \int_{E_g}^{\infty}\frac{E^2}{\exp[(E-eV_2)/k_{\mathrm{B}}T_c]-1}\mathrm{d}E\right], \tag{7}$$

where V_2 is the voltage output of the TPV cell.

According to equations (6) and (7), the power output densities P_{TIG} and P_{TPV} of the TIG and TPV cell are, respectively, given by

$$P_{\mathrm{TIG}} = j_{\mathrm{TIG}}V_1 \tag{8}$$

and

$$P_{\mathrm{TPV}} = j_{\mathrm{TPV}}V_2. \tag{9}$$

The power output density of the TIPV converter can be expressed as

$$P = P_{\mathrm{TIG}} + P_{\mathrm{TPV}}. \tag{10}$$

The net energy flux Q_e carried by the electron flux in the TIG and the net energy flux Q_h of photon flux absorbed by the TPV cell are given by [1, 32, 35]

$$Q_e = j_e(\varphi_e + 2k_{\mathrm{B}}T_e) - j_g(\varphi_e + 2k_{\mathrm{B}}T_c) \tag{11}$$

and

$$Q_h = \frac{2\pi}{h^3c^2}\left[\int_{E_c}^{\infty}\frac{E^3}{\exp[E/k_{\mathrm{B}}T_e]-1}\mathrm{d}E - \int_{E_g}^{\infty}\frac{E^3}{\exp[(E-eV_2)/k_{\mathrm{B}}T_c]-1}\mathrm{d}E\right]. \tag{12}$$

In equation (12), the first term represents the energy flux of the photons flowing out of the emitter through the filter, and the second term represents the energy flux from the PV cell because of the radiative recombination. Based on equations (10)–(12), the efficiency of the TIPV converter may be expressed as

$$\eta = P/(Q_e + Q_h). \tag{13}$$

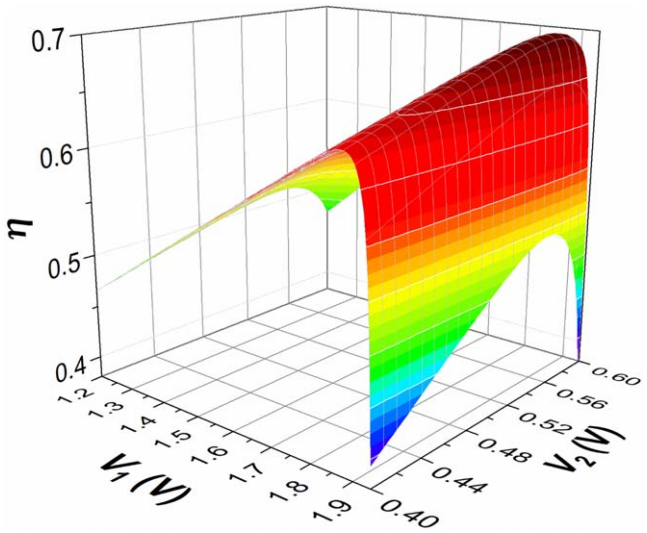

Figure 2. 3D graph of the efficiency η of the TIPV converter varying with voltages V_1 and V_2.

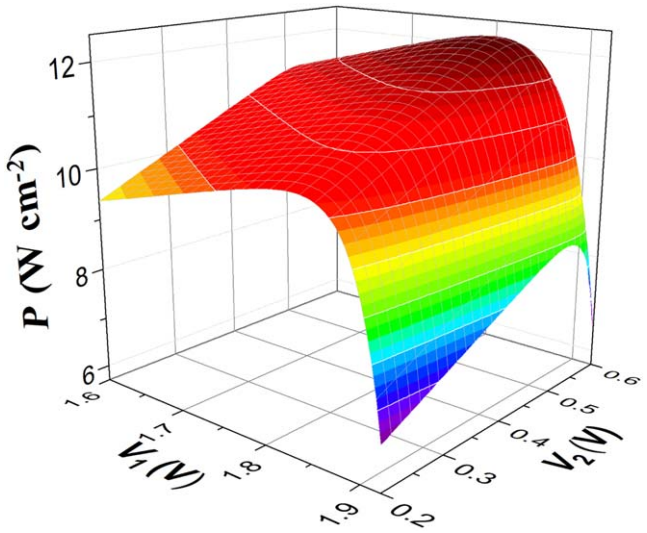

Figure 3. 3D graph of the power output density P of the TIPV converter varying with voltages V_1 and V_2.

When the TIG is not coupled with the TPV cell and is an individual device, the emitter of the TIG also emits electrons and photons simultaneously. In such a case, the net energy flux of photons Q_h' emitted from the emitter in the isolated TIG is written as [32, 37, 38]

$$Q_h' = \frac{2\pi}{h^3c^2}\left[\int_{E_C}^{\infty}\frac{E^3}{\exp[E/k_{\mathrm{B}}T_e]-1}\mathrm{d}E - \int_{0}^{\infty}\frac{E^3}{\exp[E/k_{\mathrm{B}}T_c]-1}\mathrm{d}E\right], \tag{14}$$

The second term expresses the energy flux resulting from the thermal radiation of the collector. In the single TIG, the total energy output density of the emitter should be $Q_e + Q_h'$, while the power output density is the same as that of the TIG

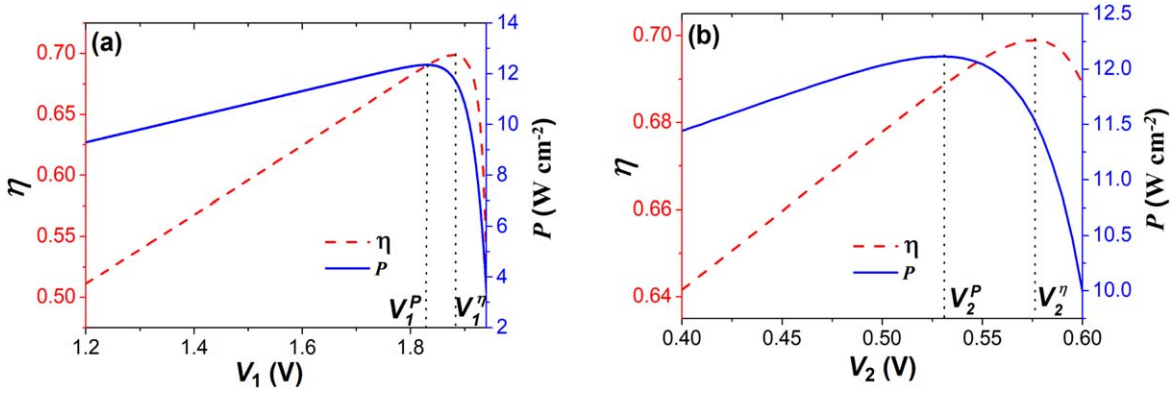

Figure 4. The optimal curves of the efficiency and power output density varying with voltages (a) V_1 and (b) V_2.

in the coupling system. Thus, the efficiency of the single TIG may be defined as

$$\eta_{\mathrm{TIG}} = P_{\mathrm{TIG}}/(Q_e + Q_h'). \tag{15}$$

When the TPV cell is a separate device, the ideal heat emitter that only radiates photons is usually used [31, 34–37]. In the single TPV cell, the total energy output density of the emitter is Q_h, and the power output density is the same as that of the TPV cell in the coupling system. Thus, the efficiency of the single TPV cell may be defined as

$$\eta_{\mathrm{TPV}} = P_{\mathrm{TPV}}/Q_h. \tag{16}$$

4. Results and discussions

In the following discussion, parameters $T_e = 1500$ K, $T_c = 300$ K, $\varphi_e = 2.3$ eV, and $E_c = E_g = 0.7$ eV are chosen. These parameters remain the same unless otherwise stated. It is worth noting that the value of φ_e is given and the value of φ_c is determined by φ_e and V_1. When the power density and the efficiency attain their respective maxima, one can determine the optimum values of V_1 and the corresponding values of φ_c. By using equations (13), (15) and (16), one can plot the three dimensional graphs of the efficiency and the power output density of the TIPV converter versus the voltages V_1 and V_2, as shown in figures 2 and 3, respectively. Figure 2 shows that there exists a maximum value $\eta_{\max}$ of the efficiency η when V_1 and V_2 attain some certain values, which are referred to as their respective optimum values and represented by V_1^η and V_2^η. According to the optimal value of V_1, the work function of graphene is required to be lower than 1 eV. Thus, one should do one's best to reduce the work function of graphene to satisfy the optimal design of TIPV converters. The maximum power density $P_{\max}$ and the corresponding optimum voltages V_1^P and V_2^P can be observed in figure 3.

In order to clearly illustrate the effects of each voltage on the performance of the TIPV converter, the optimal curves of the power output density and efficiency varying with (a) V_1 and (b) V_2 are shown in figure 4, where V_2 and V_1 has been, respectively, optimized in (a) and (b). Figure 4 shows more clearly that $V_1^P < V_1^\eta$ and $V_2^P < V_2^\eta$. According to figure 4, we

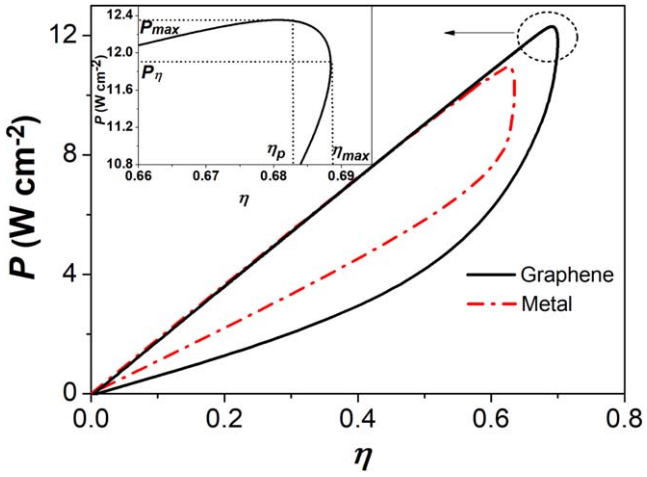

Figure 5. The optimal curve of the power output density varying with the efficiency.

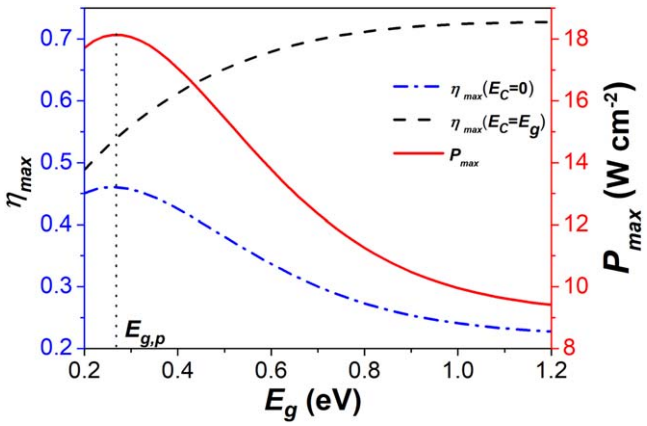

Figure 6. The optimal curves of the maximum efficiency and power output density of the TIPV converter varying with the band gap energy E_g, where the voltages V_1 and V_2 have been optimized.

can further obtain the characteristic curves between the efficiency and the power output density for the given values of other parameters, as shown in figure 5, where η_P is the efficiency corresponding to the maximum power output density and P_η is the power output density corresponding to the

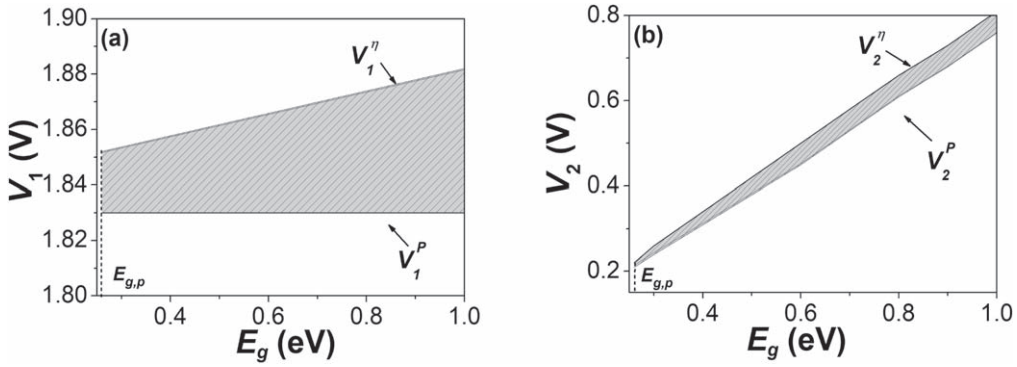

Figure 7. The curves of voltages (a) V_1 and (b) V_2 varying with the band gap energy E_g.

maximum efficiency. Figure 5 shows that the optimum ranges of P and η should be

$$P_\eta \leqslant P \leqslant P_{\max} \tag{17}$$

and

$$\eta_p \leqslant \eta \leqslant \eta_{\max}. \tag{18}$$

Figure 5 indicates that the state of $P_{\max}$ is very close to that of $\eta_{\max}$. That is to say, the optimally operating region of the TIPV converter is very small. In the design of practical devices, one should pay special attention to this problem to avoid the operation state falling in the non-optimized region. To clarify the advantages of the TIPV converter with a graphene-based anode, the optimum characteristic curve between η and P of the TIPV converter utilizing a metal anode with the same work function is also plotted, as shown by the dashed dot curve in figure 5. For the TIPV converter with a metal anode, j_g in equation (11) is replaced by the analog of equation (5) for T_c and φ_c. It is found from the curves in figure 5 that in the optimal region of the TIPV converter, the performance of the TIPV converter with a graphene-based anode is obviously better than that with a metal anode.

It is worth noting that the optimal performance of the TIPV converter closely relies on the band gap energy E_g and the cut-off energy E_c. For two limit cases of $E_c = 0$ and $E_c = E_g$, figure 6 shows the curves of the maximum efficiency $\eta_{\max}$ varying with E_g, where the voltages V_1 and V_2 have been optimized. When $E_c = 0$, the filter loses its role and all photons will go through the filter. When $E_c = E_g$, the photons through the filter are not smaller than the band gap E_g of the PV cell and will be absorbed by the PV cell to convert into electrical energy. The photons with energies below E_g are reflected by the filter and absorbed by the emitter. The spectral selectivity is implemented through the use of the energy filter, which can efficiently mitigate the photon absorption losses. It is seen from equation (12) that the heat flow Q_h absorbed by the photon flux in the TPV cell monotonically decreases as E_c increases, so that $\eta_{\max}$ is a monotonically increasing function of E_c. When $E_c = E_g$, the performance of the TIPV converter is best. It shows clearly that the use of a filter can effectively enhance the maximum efficiency of the TIPV converter. It is observed from figure 6 that when $E_c = E_g$, $\eta_{\max}$ is a monotonically increasing function of E_g. It is found from equations (6)–(10) that P is

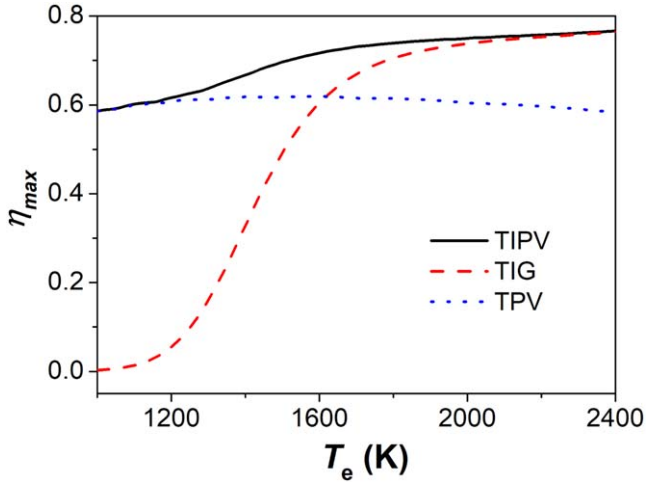

Figure 8. The maximum efficiency of the TIPV converter as a function of the emitter temperature T_e. The dash and dot curves indicate the maximum efficiencies of the TIG and TPV cell operating at the same emitter temperatures.

determined by E_g. Thus, $P_{\max}$ as a function of E_g is also indicated in figure 6. With the increase of E_g, the amount of the absorbed photons is reduced, which leads to the decrease of the short circuit current. However, the open circuit voltage is enhanced as E_g increases. As a result, $P_{\max}$ is not a monotonic function of E_g. When $E_g < E_{g,P}$, both $\eta_{\max}$ and $P_{\max}$ decrease simultaneously with the decrease of E_g. Thus, the optimal region of E_g should be

$$E_g \geqslant E_{g,P}. \tag{19}$$

The four parameters V_1^P, V_1^η, V_2^P, and V_2^η obtained from figure 4 are dependent on E_g. Figure 7 further shows these parameters as functions of E_g. To make the TIPV converter operate in the optimum regions mentioned by equations (17) and (18), the voltage outputs V_1 and V_2 must be controlled in the optimal regions described by the following equations, i.e.

$$V_1^P \leqslant V_1 \leqslant V_1^\eta \tag{20}$$

and

$$V_2^P \leqslant V_2 \leqslant V_2^\eta. \tag{21}$$

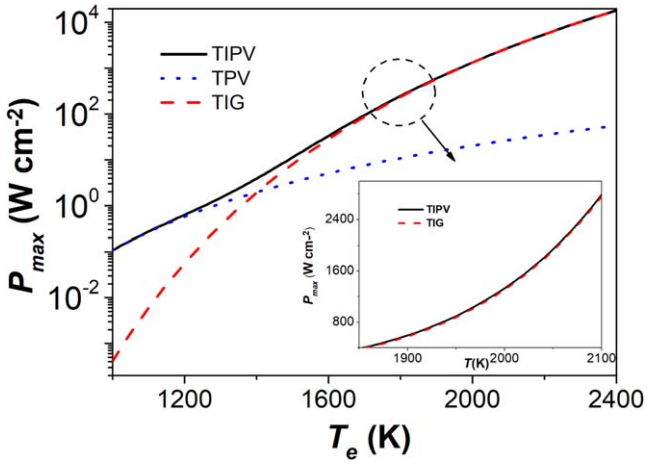

Figure 9. The maximum power output density of the TIPV converter as a function of the emitter temperature T_e. The dash and dot curves indicate the maximum power output density of the single TIG and TPV cell operating at the same emitter temperatures.

Obviously, $V_1{}^P$ and $V_1{}^\eta$ are the lower and upper bounds of the optimized voltage V_1, and $V_2{}^P$ and $V_2{}^\eta$ are the lower and upper bounds of the optimized voltage V_2.

For the purpose of illustrating the advantages of the TIPV converter, the optimal performances of the TIPV converter, TIG, and TPV cell under the differently operating conditions are further compared. Figures 8 and 9 show the maximum efficiencies and power output densities of the TIPV converter, TIG, and TPV cell operating at different emitter temperatures, where V_1 and V_2 have been optimized. It is observed from figures 8 and 9 that at low temperatures below 1200 K, $P_{\max}$ of the TIPV converter are close to those of the TPV cell, because the electron flux in the coupling device is small. The TIPV converter is not obvious superior to the TPV cell. At high temperatures over 2200 K, $P_{\max}$ and $\eta_{\max}$ of the TIPV converter are close to those of the TIG, because the electric current generated by the emitted electrons is much larger than that generated by the emitted photons. The TIPV converter is not obvious superior to the TIG. For the temperature range of 1200–2200 K, $P_{\max}$ and $\eta_{\max}$ of the TIPV converter are significantly greater than those of the TIG or TPV cell operating at the same emitter temperatures. This shows clearly that only at the suitable temperatures mentioned above, especially for the temperature of about 1300–1900 K, it is meaningful to design the TIPV converters. In addition, comparing figures 8 and 9 with figures 5 and 2 in [1], respectively, one can find that the optimal power output density and efficiency obtained by the TIPV converter with a graphene-based anode dramatically exceed those with a metal anode [1].

5. Conclusions

We have updated the model of a TIPV converter by replacing a metal anode with a graphene-based anode and optimized the systemic performance. Some significant results achieved are listed as follows.

(i) The maximum power output density and efficiency of the TIPV converter are calculated. The optimally working regions of the TIPV converter are determined.
(ii) The use of a filter can effectively enhance the maximum efficiency of the TIPV converter.
(iii) The characteristic curves of η and P of the TIPV converter with a graphene-based anode are compared with those with a metal anode [1]. Results show that the performance of the former is obviously superior to that of the latter.
(iv) In the temperature range of 1300–1900 K, $P_{\max}$ and $\eta_{\max}$ of the TIPV converter are significantly greater than those of the TIG or TPV cell operating at the same emitter temperatures.
(v) The optimal performance of the TIPV converter relies on the band gap energy of the cell. The semiconductor materials with the band gap energy below $E_{g,P}$ are not suitable for TIPV converters.

Acknowledgments

This work has been supported by the National Natural Science Foundation (Grant No. 11805159) and the Fundamental Research Fund for the Central Universities (No. 20720180011), People's Republic of China.

ORCID iDs

Zhimin Yang https://orcid.org/0000-0003-0681-0445
Shanhe Su https://orcid.org/0000-0001-6076-1176

References

[1] Datas A 2016 Hybrid thermionic-photovoltaic converter *Appl. Phys. Lett.* **108** 143503
[2] Chubb D 1985 Thermionic-photovoltaic energy converter *US Patent* 4,528,417
[3] Zak J and Wade J 2011 Hybrid photovoltaic and thermionic energy converter *US Patent App.* 12/590, 304
[4] Houston J 1959 Theoretical efficiency of the thermionic energy converter *J. Appl. Phys.* **30** 481–7
[5] Hatsopoulos G and Gyftopoulos E 1979 Thermionic energy conversion *Theory, Technology, and Application* Vol II (Cambridge, MA: MIT Press)
[6] Wilson V 1959 Conversion of heat to electricity by thermionic emission *J. Appl. Phys.* **30** 475–81
[7] Khalid K, Leong T and Mohamed K 2016 Review on thermionic energy converters *IEEE Trans. Electron Dev.* **63** 2231–41
[8] Li X, Zhu Y, Cai W, Borysiak M, Han B, Chen D, Piner R, Colombo L and Ruoff S R 2009 Transfer of large-area graphene films for high-performance transparent conductive electrodes *Nano Lett.* **9** 4359–63
[9] Arco L G D, Zhang Y, Schlenker C W, Koungmin R, Thompson M E and Zhou C 2010 Continuous, highly flexible, and transparent graphene films by chemical vapor deposition for organic photovoltaics *ACS Nano* **4** 2865–73

[10] Sheehy D E and Schmalian J 2009 Optical transparency of graphene as determined by the fine-structure constant *Phys. Rev.* B **80** 193411
[11] Shi Y M, Kim K K, Reina A, Hofmann M, Li L and Kong J 2010 Work function engineering of graphene electrode via chemical doping *ACS Nano* **4** 2689–94
[12] Yu Y, Zhao Y, Ryu S, Brus L E, Kim K S and Kim P 2009 Tuning the graphene work function by electric field effect *Nano Lett.* **9** 3430–4
[13] Giovannetti G, Khomyakov P A, Brocks G, Karpan V M, Brink J V D and Kelly P J 2008 Doping graphene with metal contacts *Phys. Rev. Lett.* **101** 026803
[14] Voss J, Vojvodic A, Chou S, Chou S, Howe R T and Pedersen F A 2014 Inherent enhancement of electronic emission from hexaboride heterostructure *Phys. Rev.* A **2** 024004
[15] Hovel H J 1976 Transparency of thin metal films on semiconductor substrates *J. Appl. Phys.* **47** 4968–70
[16] Yuan H, Riley D C, Shen Z, Pianetta P A, Melosh N A and Roger T 2017 Back-gated graphene anode for more efficient thermionic energy converters *Nano Energy* **32** 67–72
[17] Liang S and Ang L K 2015 Electron thermionic emission from graphene and a thermionic energy converter *Phys. Rev. Appl.* **3** 014002
[18] Zhang X, Pan Y and Chen J 2017 Parametric optimum design of a graphene-based thermionic energy converter *IEEE Trans. Electron Dev.* **64** 4594–8
[19] Yuan H, Chang S, Bargatin I, Wang N, Riley D, Wang H, Schwede J, Provine J and Eric P 2015 Engineering ultra-low work function of graphene *Nano Lett.* 6475–80
[20] Basu S, Chen Y and Zhang Z 2007 Microscale radiation in thermophotovoltaic devices—a review *Int. J. Energy Res.* **31** 689–716
[21] Te-Kao W 1997 Infrared filters for high-efficiency thermovoltaic devices *Microw. Opt. Technol. Lett.* **15** 9–12
[22] Lei M and Hong Y 2010 New development of one-dimensional Si/SiO_2 photonic crystals filter for thermophotovoltaic applications *Renew. Energy* **35** 249–56
[23] Mostafa S, Rafat N and El-Naggar S 2012 One-dimensional metallic-dielectric (Ag/SiO_2) photonic crystals filter for thermophotovoltaic applications *Renew. Energy* **45** 245–50
[24] Pop E, Varshney V and Roy A K 2012 Thermal properties of graphene: fundamentals and applications *MRS Bull.* **37** 1273–81
[25] Liang S, Liu B, Hu W, Zhou K and Ang L K 2017 Thermionic energy conversion based on graphene van der waals heterostructures *Sci. Rep.* **7** 46211
[26] Wallace P R 1947 The band theory of graphite *Phys. Rev.* **71** 622
[27] Castro Neto A H, Guinea F, Peres N M R, Novoselov K S and Geim A K 2009 The electronic properties of graphene *Rev. Mod. Phys.* **81** 109
[28] Misra S, Upadhyay K M and Mishra S K 2017 Thermionic emission from monolayer graphene, sheath formation and its feasibility towards thermionic converters *J. Appl. Phys.* **121** 065102
[29] Gerstenmaiera Y and Wachutka G 2019 Thermionic emission laws for general electron dispersion relations and band structure data *J. Appl. Phys.* **125** 215105
[30] Datas A and Algora C 2010 Detailed balance analysis of solar thermophotovoltaic systems made up of single junction photovoltaic cells and broadband thermal emitters *Energ. Mater. Sol. Cells* **94** 2137–47
[31] Zenker M, Heinzel A, Stollwerck G, Ferber J and Luther J 2001 Efficiency and power density potential of combustion-driven thermophotovoltaic systems using GaSb photovoltaic cells *IEEE Trans. Electron Dev.* **48** 367–76
[32] Dong Q, Liao T, Yang Z, Chen X and Chen J 2017 Performance characteristics and parametric choices of a solar thermophotovoltaic cell at the maximum efficiency *Energy Convers. Manage.* **136** 44–9
[33] Chubb D 2007 *Fundamentals of Thermophotovoltaic Energy Conversion* (Amsterdam: Elsevier)
[34] Liao T, Chen X, Yang Z, Lin B and Chen J 2016 Parametric characteristics of a solar thermophotovoltaic system at the maximum efficiency *Energy Convers. Manage.* **126** 205–9
[35] Yang Z, Wang J, Chen X and Lin G 2018 Parametric optimum design criteria of a thermophotovoltaic cell *Environ. Prog. Sustain.* **37** 513–7
[36] Datas A, Chubb D L and Veeraragavan A 2013 Steady state analysis of a storage integrated solar thermophotovoltaic (SISTPV) system *Sol. Energy* **96** 33–45
[37] Wang Y, Su S, Lin B and Chen J 2013 Parametric design criteria of an irreversible vacuum thermionic generator *J. Appl. Phys.* **114** 053502
[38] Tervo E, Bagherisereshki E and Zhang Z 2018 Near-field radiative thermoelectric energy converters: a review *Frontiers Energy* **12** 5–21